

A 10^{10} SOLAR MASS FLOW OF MOLECULAR GAS IN THE A1835 BRIGHTEST CLUSTER GALAXY

B. R. MCNAMARA^{1,2,3}, H. R. RUSSELL¹, P. E. J. NULSEN³, A. C. EDGE⁴, N. W. MURRAY⁵, R. A. MAIN¹, A. N. VANTYGHM¹,
F. COMBES⁶, A. C. FABIAN⁷, P. SALOME⁶, C. C. KIRKPATRICK¹, S. A. BAUM⁸, J. N. BREGMAN⁹, M. DONAHUE¹⁰, E. EGAMI¹¹,
S. HAMER⁵, C. P. O'DEA⁸, J. B. R. OONK¹², G. TREMBLAY¹³, AND G. M. VOIT¹⁰

¹ Department of Physics and Astronomy, University of Waterloo, Waterloo, Canada

² Perimeter Institute for Theoretical Physics, Waterloo, Canada

³ Harvard-Smithsonian Center for Astrophysics, Cambridge, MA 02138, USA

⁴ Department of Physics, Durham University, Durham DH1 3LE, UK

⁵ Canadian Institute for Theoretical Astrophysics, University of Toronto, 60 St. George Street, Toronto, M5S 3H8 ON, Canada

⁶ L'Observatoire de Paris, 61 Av. de L'Observatoire, F-75014 Paris, France

⁷ Institute of Astronomy, Madingley Road, Cambridge CB3 0HA, UK

⁸ School of Physics and Astronomy, Rochester Institute of Technology, Rochester, NY 14623, USA

⁹ Department of Astronomy, University of Michigan, 500 Church Street, Ann Arbor, MI 48109, USA

¹⁰ Department of Physics and Astronomy, Michigan State University, 567 Wilson Road, East Lansing, MI 48824, USA

¹¹ Steward Observatory, University of Arizona, 933 N. Cherry Avenue, Tucson, AZ 85721, USA

¹² Netherlands Institute for Radio Astronomy, Postbus 2, 7990 AA Dwingeloo, The Netherlands

¹³ European Southern Observatory, Karl-Schwarzschild-Strasse 2, D-85748 Garching, Germany

Received 2013 August 29; accepted 2014 February 5; published 2014 March 25

ABSTRACT

We report ALMA Early Science observations of the A1835 brightest cluster galaxy (BCG) in the CO (3–2) and CO (1–0) emission lines. We detect $5 \times 10^{10} M_{\odot}$ of molecular gas within 10 kpc of the BCG. Its ensemble velocity profile width of $\sim 130 \text{ km s}^{-1}$ FWHM is too narrow for the molecular clouds to be supported in the galaxy by dynamic pressure. The gas may instead be supported in a rotating, turbulent disk oriented nearly face-on. Roughly $10^{10} M_{\odot}$ of molecular gas is projected 3–10 kpc to the northwest and to the east of the nucleus with line-of-sight velocities lying between -250 km s^{-1} and $+480 \text{ km s}^{-1}$ with respect to the systemic velocity. The high-velocity gas may be either inflowing or outflowing. However, the absence of high-velocity gas toward the nucleus that would be expected in a steady inflow, and its bipolar distribution on either side of the nucleus, are more naturally explained as outflow. Star formation and radiation from the active galactic nucleus (AGN) are both incapable of driving an outflow of this magnitude. The location of the high-velocity gas projected behind buoyantly rising X-ray cavities and favorable energetics suggest an outflow driven by the radio AGN. If so, the molecular outflow may be associated with a hot outflow on larger scales reported by Kirkpatrick and colleagues. The molecular gas flow rate of approximately $200 M_{\odot} \text{ yr}^{-1}$ is comparable to the star formation rate of $100\text{--}180 M_{\odot} \text{ yr}^{-1}$ in the central disk. How radio bubbles would lift dense molecular gas in their updrafts, how much gas will be lost to the BCG, and how much will return to fuel future star formation and AGN activity are poorly understood. Our results imply that radio-mechanical (radio-mode) feedback not only heats hot atmospheres surrounding elliptical galaxies and BCGs, but it is able to sweep higher density molecular gas away from their centers.

Key words: galaxies: active – galaxies: clusters: general – galaxies: clusters: individual (A1835) – galaxies: star formation – ISM: jets and outflows – ISM: molecules

Online-only material: color figures

1. INTRODUCTION

Brightest cluster galaxies (BCGs) are the largest and most luminous galaxies in the universe. Like normal elliptical galaxies, their stellar populations are usually old and dormant. The BCGs residing in cooling flow clusters are exceptional (Fabian 1994). Fueled by unusually large reservoirs of cold molecular clouds (Edge 2001; Salomé & Combes 2003), many form stars at rates of several to several tens of solar masses per year (O’Dea et al. 2008). Extreme objects, such as the Phoenix and the A1835 BCGs, are forming stars at rates upward of $100 M_{\odot} \text{ yr}^{-1}$ (McDonald et al. 2012; McNamara et al. 2006, hereafter M06).

The origin of star formation in a population of normally “red and dead” galaxies is not entirely clear. In some instances, BCGs may be rejuvenated by collisions with gas-rich galaxies. However, wet mergers must be uncommon in BCGs due to a dearth of gas-rich donor galaxies in cluster cores. A wealth of data suggests that molecular clouds and young stars forming in BCGs are usually fueled instead by gas cooling from hot

atmospheres. For example, bright nebular emission and young stars are observed preferentially when the central cooling time of a cluster atmosphere falls below ~ 1 Gyr (Heckman 1981; Hu et al. 1985). Furthermore, high-resolution X-ray imaging has since revealed that nebular emission and star formation appear at a sharp threshold or transition as the central cooling time falls below $\sim 5 \times 10^8$ yr (Rafferty et al. 2008; Cavagnolo et al. 2008). Voit and others have attributed this threshold to cooling instabilities and thermal conduction in hot atmospheres (Voit et al. 2008; Voit 2011; Gaspari et al. 2012; Guo & Mathews 2013).

Despite strong indications that cold clouds are condensing out of hot atmospheres, only a few percent of the mass expected to cool actually does so (Peterson & Fabian 2006). Feedback from active galactic nuclei (AGNs) is almost certainly suppressing cooling below the levels expected in an unimpeded cooling flow (reviewed by McNamara & Nulsen 2007, 2012; Fabian 2013). So-called radio-mode or radio-mechanical feedback operates primarily on the hot, volume-filling atmosphere. The energy

released by radio AGNs increases the entropy of the hot gas (O’Neill & Jones 2010) and drives the most rapidly cooling gas outward, thereby regulating the cooling rate, the star formation rate, and the power output of the AGN itself.

Despite the widely held view that radio-mechanical feedback maintains BCGs and giant elliptical galaxies in dormancy, little is known of its effect on molecular gas. This is a potentially significant issue because the rate of cold accretion onto AGNs may be a crucial element of an operational feedback loop (Pizzolato & Soker 2010; Gaspari et al. 2013). Radio jets are known to interact with nebular gas surrounding them (e.g., Villar-Martín et al. 2006; Nesvadba et al. 2006), which are likely to be the ionized skins of molecular clouds (Wilman et al. 2006; Emonts et al. 2013). Furthermore, blueshifted absorption lines of neutral atomic hydrogen have been observed toward several radio galaxies (Morganti et al. 2005, 2013), indicating that radio jets couple effectively to cold clouds and are able to drive them out at high speed. NGC 1275 in the Perseus cluster is a striking example of radio lobes interacting with molecular clouds (Salomé et al. 2006, 2011). Both inflow and outflow are observed in what appears to be a molecular “fountain” (Lim et al. 2008). A1835, discussed here, may be similar to Perseus.

Here we examine the effects of feedback on the molecular gas located near the nucleus of the A1835 BCG. The BCG contains upward of $\simeq 5 \times 10^{10} M_{\odot}$ of molecular gas (Edge 2001) and star formation proceeding at a rate of between $100\text{--}180 M_{\odot} \text{ yr}^{-1}$ (M06). The AGN launched a pair of cavities into its hot atmosphere a few 10^7 yr ago, each of which is 20 kpc in diameter and projects roughly 20 kpc from the nucleus. The AGN’s radio synchrotron luminosity, $3.6 \times 10^{41} \text{ erg s}^{-1}$, is dwarfed by its mechanical power, $L_{\text{mec}} \simeq 10^{45} \text{ erg s}^{-1}$ (M06), which is typical of radio AGNs (Birzan et al. 2008). A1835 is an archetypal cooling flow regulated by radio-mode feedback. The ALMA Early Science observations reported here and in a companion paper on A1664 (Russell et al. 2014) explore for the first time at high resolution the relationships between molecular gas, star formation, and radio AGN feedback. At the emission line redshift $z = 0.252$ (Crawford et al. 1999), 1 arcsec = 3.9 kpc.

2. OBSERVATIONS

We obtained Early Science observations of the BCG with ALMA at 92 GHz (band 3) and 276 GHz (band 7). At the cluster’s redshift, the bands are sensitive to the carbon monoxide molecule’s $J = 1,0$ and $J = 3,2$ rotational transitions, respectively. The exposures, totaling 60 minutes in band 3 and 60 minutes in band 7, were made between 2012 March 27 and 2012 April 24. The extended array available for Cycle 0 included on average twenty 12 m dishes, which provided a spatial resolution of 0.5 arcsec in the CO (3–2) transition and 1.5 arcsec at the CO (1–0) transition. Baselines extended to ~ 400 m. This combination yielded a sharp image of the molecular gas near the nucleus at CO (3–2) and sensitivity on larger spatial scales at CO (1–0). A bandwidth of 1.875 GHz per spectral window and two spectral windows per sideband provided a total frequency range of ~ 7 GHz. We used a spectral resolution of 0.488 MHz per channel. Channels were binned together to improve the signal-to-noise ratio, yielding a final resolution of 20 km s^{-1} . The quasar 3C 279 was observed for bandpass calibration, and observations of Mars and Titan provided absolute flux calibration. Observations switched from A1835 to the nearby phase calibrator J1332+0200 every ~ 10 minutes.

The observations were calibrated using the CASA software (version 3.3) following the detailed processing scripts provided

by the ALMA science support team. The continuum-subtracted images were reconstructed using the CASA task CLEAN assuming Briggs weighting with a robustness parameter of 0.5 and with a simple polygon mask applied to each channel. This provided a synthesized beam of $1''.7 \times 1''.3$ at a P.A. of $-84^{\circ}.1$ at CO (1–0) and $0''.60 \times 0''.48$ at a P.A. of $-80^{\circ}.0$ at CO (3–2). The rms noise in the line-free channels was $0.6 \text{ mJy beam}^{-1}$ at CO (1–0) and $1.6 \text{ mJy beam}^{-1}$ at CO (3–2). Images of the continuum emission were also produced with CLEAN by averaging channels free of any line emission. A central continuum source is detected in both bands at position 140102.083, +025242.649 with fluxes $1.26 \pm 0.03 \text{ mJy}$ in band 3 and $0.7 \pm 0.1 \text{ mJy}$ in band 7. The millimeter-continuum source position coincides with the Very Large Array radio nucleus position (e.g., M. T. Hogan et al., in preparation). The millimeter-continuum flux is consistent to within a factor of two with being synchrotron emission from a central, low-luminosity radio AGN with a spectral energy distribution¹⁴ of spectral index $\alpha \propto 0.84$ (Hogan et al., in preparation).

3. ANALYSIS

3.1. Spectra

The total CO (3–2) and CO (1–0) spectra are presented in Figure 1. The CO emission is centered within $\sim 100 \text{ km s}^{-1}$ of the nebular emission line redshift (Crawford et al. 1999). Each spectral profile was fitted with a single Gaussian after the continuum was subtracted. The emission integral at CO (1–0) is $3.6 \pm 0.2 \text{ Jy km s}^{-1}$. The molecular gas mass was calculated as

$$M_{\text{mol}} = 1.05 \times 10^4 X_{\text{CO}} \left(\frac{1}{1+z} \right) \left(\frac{S_{\text{CO}} \Delta v}{\text{Jy km s}^{-1}} \right) \left(\frac{D_L}{\text{Mpc}} \right)^2 M_{\odot}. \quad (1)$$

This expression yields a total molecular gas mass of $4.9 \pm 0.2 \times 10^{10} M_{\odot}$. The conversion factor between CO and molecular gas, $X_{\text{CO}} = 2 \times 10^{20} \text{ cm}^{-2} (\text{K km s}^{-1})^{-1}$, is the average Galactic value (Bolatto et al. 2013; Narayanan et al. 2012). The primary line at zero velocity has a Gaussian profile full-width at half maximum, $\text{FWHM} = 130 \pm 5 \text{ km s}^{-1}$, after correcting for instrumental broadening. This width is 5–6 times smaller than would correspond to the BCG’s expected velocity dispersion $\sim 250\text{--}300 \text{ km s}^{-1}$. Molecular gas moving with a nearly isotropic velocity pattern cannot be supported against collapse at such low speeds. The gas may be supported instead by rotation in a disk projected nearly face-on. The observed velocity width would then represent gas speeds out of the disk’s plane (Section 4.4).

3.2. Central Molecular Gas and Star Formation

The *R*-band and far-UV (FUV) images taken with the *Hubble Space Telescope* (O’Dea et al. 2010) are presented in Figure 2. The *R*-band image shows the BCG in relation to its molecular gas, hot atmosphere, and other neighboring galaxies. The box superposed on the image indicates the scale of the UV and CO (3–2) images presented in Figure 2. A *Chandra* X-ray image with a similar box superposed is shown in Figure 2. Most of the molecular gas lies within one arcsec (4 kpc) of the nucleus. The UV continuum emission is emerging from the sites of star formation proceeding at a rate upward of $100\text{--}180 M_{\odot} \text{ yr}^{-1}$ (M06; Egami et al. 2006; Donahue et al. 2011). No bright UV

¹⁴ For the convention $f_{\nu} \propto \nu^{-\alpha}$.

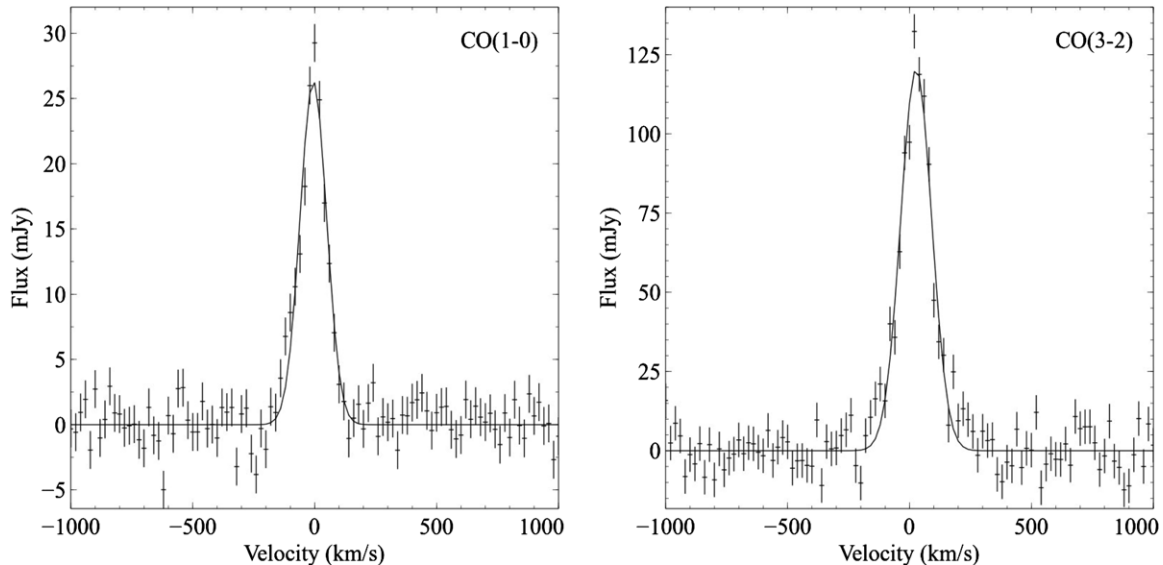


Figure 1. Spectra for CO (1–0) and CO (3–2) on the left and right, respectively. The spectra were extracted from regions measuring 6×6 arcsec.

or X-ray point source is associated with a nuclear AGN. The CO (3–2) gas coincident with the UV emission is presumably fueling star formation. The CO and UV emissions are straddled by two bright and presumably rapidly cooling X-ray emission regions oriented to the northeast and southwest of the nucleus. No CO emission is detected toward the most rapidly cooling gas. Two X-ray cavities are located a few arcsec to the northwest and southeast of the CO (3–2) emission.

Roughly half of the CO (3–2) flux is emerging from the inner half-arcsecond radius of the BCG and is unresolved. Assuming half of the central molecular gas mass and star formation lie within the same region, we find the surface densities of star formation and molecular gas to be $\log \Sigma_{\text{SFR}} = 0.87 M_{\odot} \text{ yr}^{-1} \text{ kpc}^{-2}$ and $\log \mu_{\text{CO}} = 3.2 M_{\odot} \text{ pc}^{-2}$, respectively. Based on these values, the BCG lies with normal, circumnuclear starburst galaxies on the Schmidt–Kennicutt relation (Kennicutt 1998).

3.3. Velocity Field of the Molecular Gas

We present a grid of CO (3–2) emission spectra corresponding to the grid projected onto the CO (3–2) image in Figure 3. The mean line-of-sight velocities measured with Gaussian profile fits are indicated in each grid box. The size of each grid box corresponds approximately to the FWHM of the synthesized beam. Velocity differences of a few to a few tens of km s^{-1} are observed across the central structure. No clear evidence for rotation is observed. If the CO (3–2) structure is a rotating disk, the small velocity gradients and narrow line width are consistent with it being nearly face-on.

Figure 4 is similar to Figure 3, but with a coarser grid intended to increase the signal in the outer region of the central structure. The mean line-of-sight velocities of the emission features are indicated where significant CO (3–2) is detected in emission. The tongue of gas located 1.5 arcsec to the north has a broad line profile with velocities of -15 to -60 km s^{-1} . Likewise, the tongue extending to the west is traveling at a velocity of -70 km s^{-1} with respect to the bulk of the gas. The gas in the east–southeast (bottom left) grid boxes has velocities similar in magnitude but opposite in sign (redshifted) with respect to the central emission. The north and west tongues of blueshifted

gas are oriented roughly toward the northwest X-ray cavity. The redshifted gas to the southeast is oriented roughly toward the southeast X-ray cavity. The tongues of gas appear to be dynamically decoupled from the central structure. Below, we relate this gas to the more extended molecular gas seen in CO (1–0).

We examine the molecular gas velocities on larger scales using the grid of spectra in CO (1–0) presented in Figure 5, which matches the resolution of the telescope configuration. The sky grid corresponds to spectra shown in the right panel. The contours represent CO emission, and their colors correspond to the color-coded velocity stripes superposed on the spectra. A two-dimensional Gaussian profile has been fitted to and subtracted from each channel in order to remove the central emission from the contour map.

The CO (1–0) map reveals tongues of emission projecting roughly 10 kpc to the north–northwest and southeast of the nucleus. Their orientations are similar to the smaller, tongue-like features seen in the CO (3–2) image. Molecular gas traveling at $+480 \text{ km s}^{-1}$ in the eastern box is redshifted with respect to the systemic velocity. A narrower, blueshifted gas velocity component is seen in the north and northwest boxes extending to velocities of -200 km s^{-1} . The redshifted gas contour north of the nucleus is significant only at the 2σ – 3σ level. Present as a small bump in the nuclear spectrum at a velocity of 300 km s^{-1} , it is of marginal significance and will not be discussed further.

In summary, blueshifted gas lies exclusively to the north–northwest, whereas redshifted gas lies primarily to the east–southeast. No significant high-velocity gas is observed in the northeast, southwest, and west grid boxes, nor is it observed toward the nucleus. This pattern is consistent with a broad, bipolar flow of molecular gas, which we discuss in greater detail in Section 4.3. While this interpretation accounts best for the data in hand, it is not unique. The gas may in principle have accreted with some net angular momentum that placed it on nearly circular rather than radial orbits so that the gas is in nearly ordered motion about the BCG.

The integrated flux under the redshifted and blueshifted emission profile wings are 0.4 ± 0.2 and $0.27 \pm 0.09 \text{ Jy km s}^{-1}$, respectively, giving a total flux integral of $0.7 \pm 0.2 \text{ Jy km s}^{-1}$. They correspond to a molecular hydrogen mass of $1.0 \pm 0.3 \times$

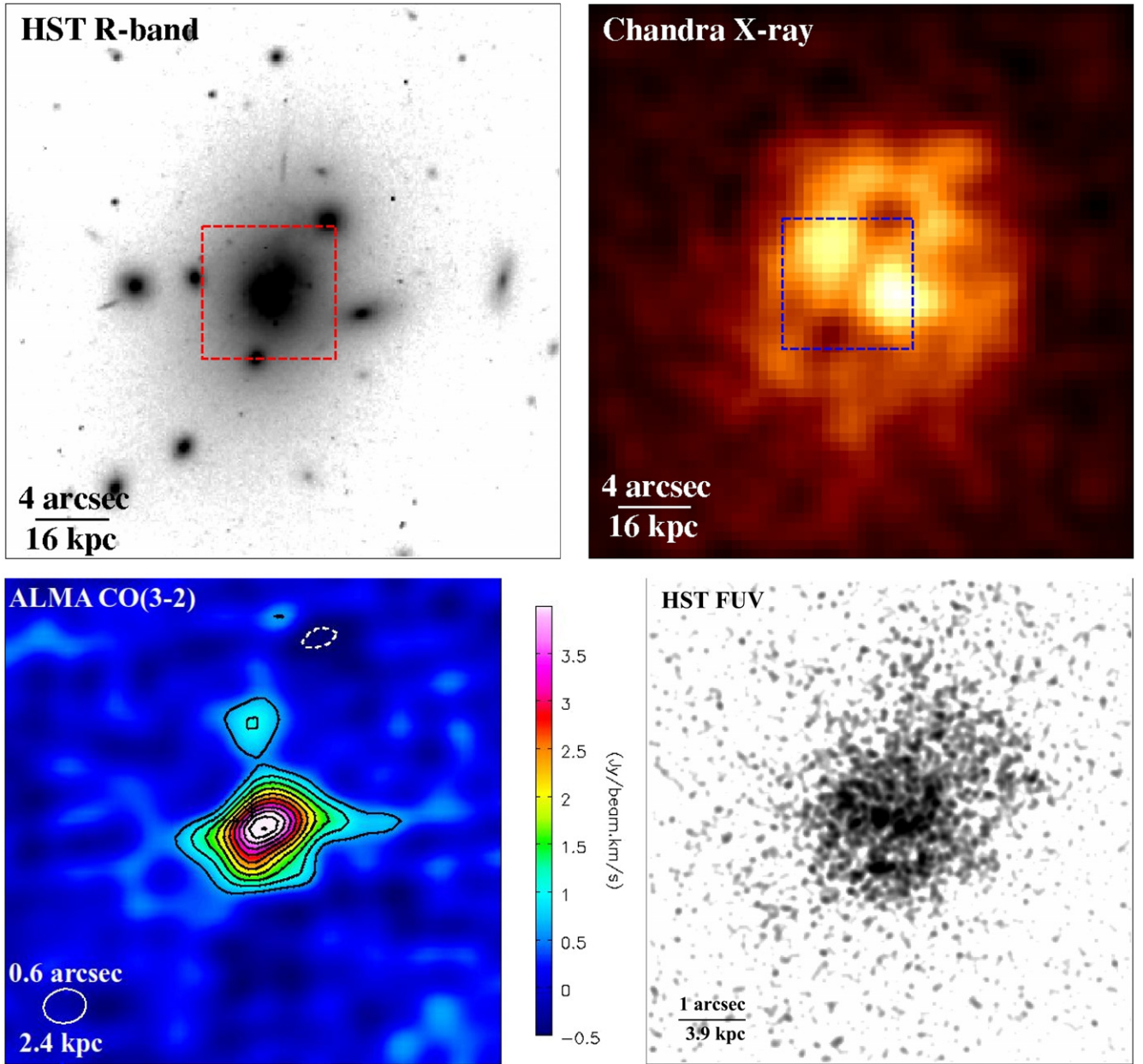


Figure 2. Upper left: *Hubble Space Telescope* F702W WFPC2 image of the BCG and surrounding galaxies in A1835. The red box indicates the scale of the CO (3–2) image at lower left. The image is sensitive to both the old and young stellar populations and accompanying line emission. Upper right: *Chandra* X-ray image of the hot atmosphere surrounding the BCG. A smooth X-ray background has been subtracted. The blue box indicates the location and scale of the CO (3–2) and UV images in the lower panels. X-ray cavities inflated by the radio AGN (M06) are seen to the northwest and southeast near the edges of the box. The bright regions to the northeast and southwest of center are the locations of gas with the shortest cooling time where the atmosphere is cooling rapidly. Lower left: CO (3–2) image. The oval at lower left indicates the beam size, shape, and scale in arcseconds and kiloparsecs. The contours represent $-3, +3, +6, +9, \dots \sigma$. Lower right: far-ultraviolet continuum image through filter F165LP ACS Solar Blind Channel. Note the absence of a nuclear point source associated with an AGN. Essentially all of the continuum is from the young stars.

(A color version of this figure is available in the online journal.)

$10^{10} M_{\odot}$. The accuracy of the integrated fluxes are sensitive to the continuum, particularly in the redshifted emission wing. A slightly higher mass is found in the redshifted component compared to the blueshifted component, indicating an asymmetric flow.

4. DISCUSSION

4.1. Bipolar Outflow or Inflow of Molecular Gas?

The high-speed molecular gas is observed in emission, so the ALMA observations alone are unable to discriminate between inflow and outflow. An inflow of molecular gas from the cooling

flow would be a natural but problematic interpretation. Gas cooling from a steady accretion flow would fall inward, reaching its highest speeds in the nucleus (Lim et al. 2008). This is not observed. Instead, the high-velocity gas is projected away from the nucleus. Assuming the CO (3–2) and CO (1–0) lines track the same gas, higher line-of-sight velocities are observed 5–10 kpc toward the northwest and southeast of the nucleus. The gas to the north–northwest is blueshifted from velocities of a few tens of km s^{-1} at radii of ~ 3 kpc to $\sim 250 \text{ km s}^{-1}$ at a radius of ~ 10 kpc. Likewise, the gas to the east–southeast is redshifted with velocities of ~ 40 – 60 km s^{-1} at ~ 3 kpc, increasing to $> 300 \text{ km s}^{-1}$ at ~ 10 kpc. The yellow wing in the

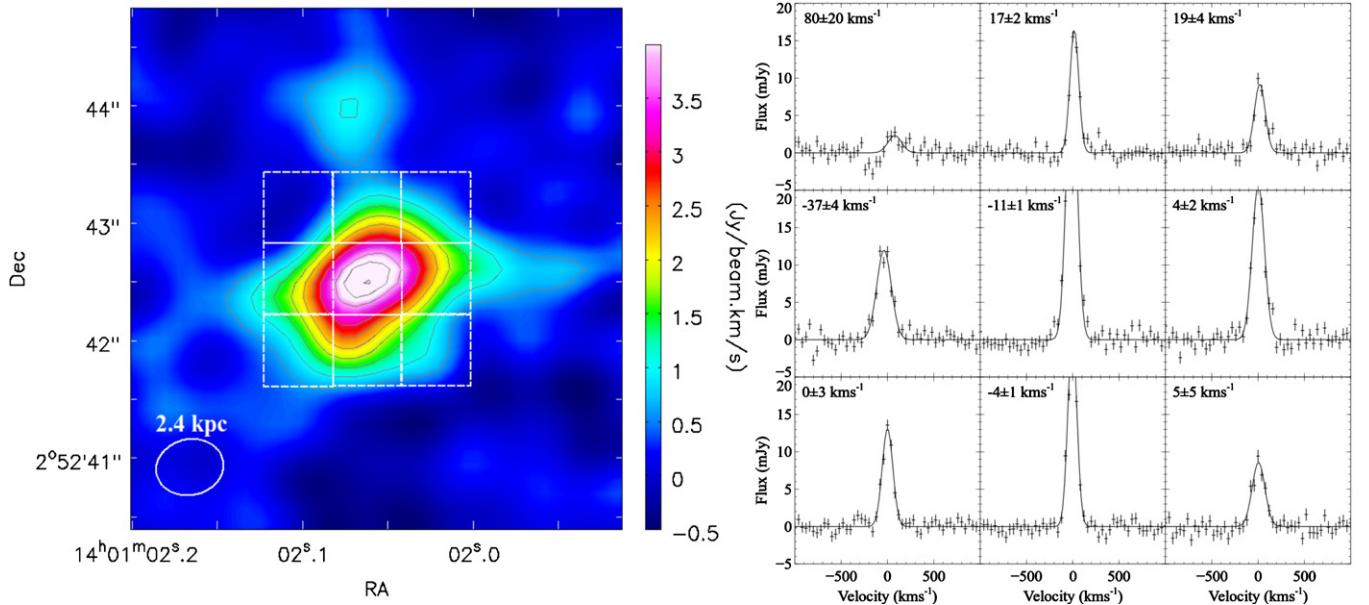


Figure 3. CO (3–2) images with a grid of apertures corresponding to the spectra shown in the right panel. The extractions are 0.6 arcsec on a side, corresponding to the resolution of the synthesized beam. The velocity centroids and their errors are indicated in each box.

(A color version of this figure is available in the online journal.)

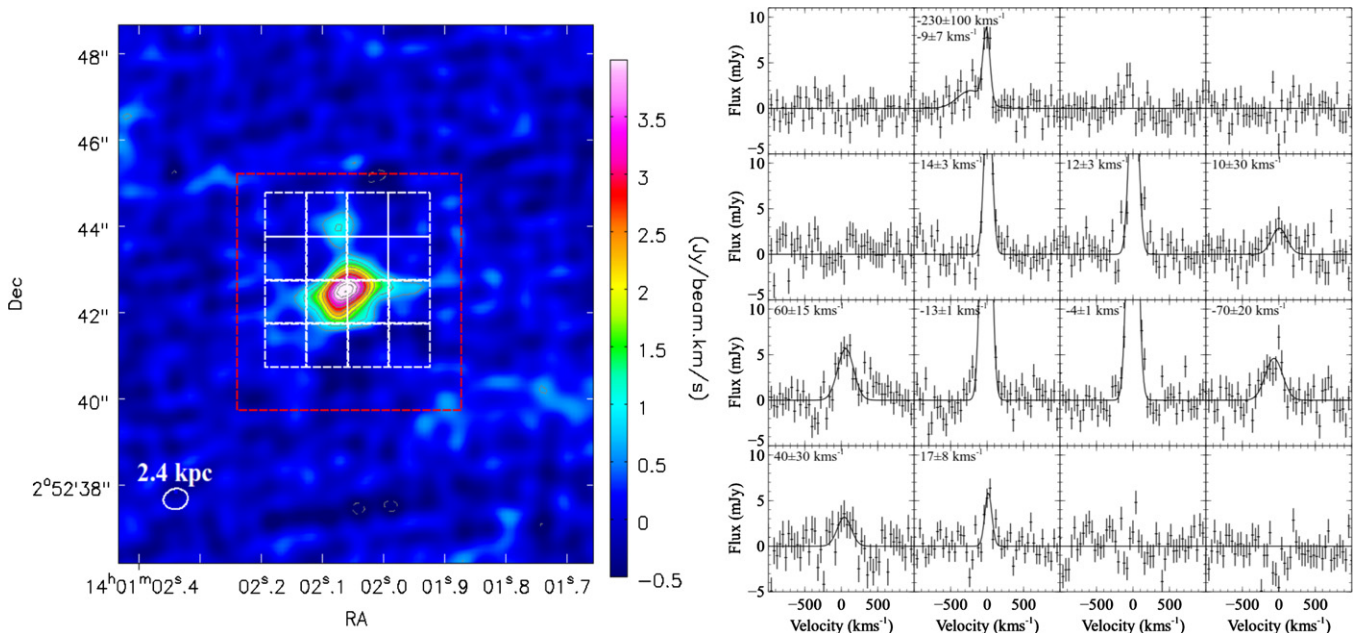


Figure 4. Similar to Figure 3, but with 1 arcsec extraction apertures that extend into the fainter outer reaches of the central gas structure. The red box corresponds to the outer edge of the grid region shown in the CO (1–0) map in Figure 5.

(A color version of this figure is available in the online journal.)

nuclear spectrum at $+250 \text{ km s}^{-1}$ strengthens as it is redshifted to higher velocities in the eastern grid box, indicating higher gas masses traveling at higher speeds.

Let us assume the gas projected 10 kpc from the nucleus with radial speeds lying between 250 and 480 km s^{-1} began its descent at rest and fell radially to its current location. We estimate its initial radius using a Hernquist law by adopting an enclosed mass within a 20 kpc radius of $1.6 \times 10^{12} M_{\odot}$ (R. A. Main et al., in preparation), and an effective radius of ~ 10 kpc. We find that this molecular gas would have achieved its radial speed had it fallen from an altitude of $\sim 20\text{--}30$ kpc. If gas is flowing steadily onto the disk, we would expect

to observe gas velocities toward the disk and nucleus lying between 600 and 800 km s^{-1} , but we do not. Molecular gas that began its journey with a significant initial velocity (imparted by turbulence or a donor galaxy) would be traveling faster. In principle, drag from the intracluster medium might slow infalling clouds more effectively closer to the cluster center. However, cloud parameters must then be finely tuned to allow the clouds to free fall at large radii while giving them terminal speeds on the order of 10 km s^{-1} at smaller radii.

We are then left with the following two scenarios: the high-speed molecular gas cooled recently from the hot atmosphere in the past 10 Myr or so and has not yet arrived in the disk,

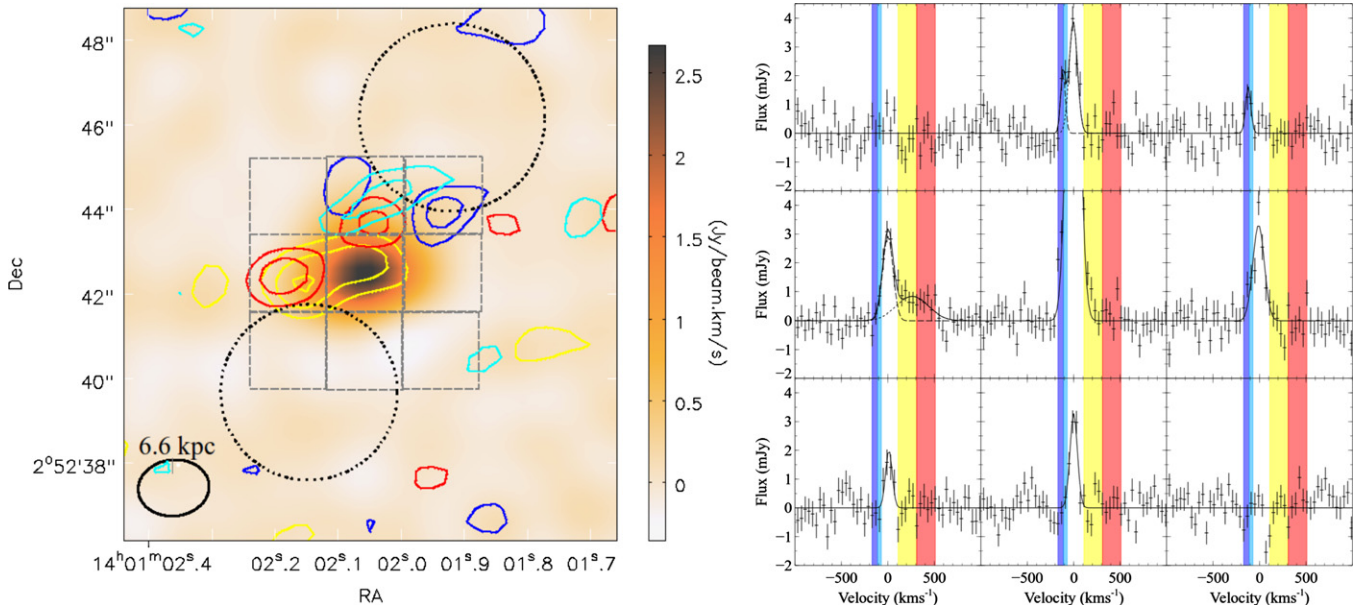


Figure 5. Left panel shows a color-scale image of CO (1–0) emission with color contours divided into separate velocity bins. The contours are integrated intensity in particular velocity ranges with $+2\sigma$, 3σ , 4σ . Dark blue (-210 to -150 km s $^{-1}$), cyan (-150 to -110 km s $^{-1}$), yellow (70 – 270 km s $^{-1}$), red (270 – 470 km s $^{-1}$). A two-dimensional Gaussian profile has been fitted to and subtracted from each channel in order to remove the central emission from the contour map. The right panel shows spectral extractions 1.8×1.8 arcsec on a side, roughly corresponding to the CO (1–0) beam size. The colors superposed on the spectra correspond to the velocity contours. This figure shows that the high-velocity molecular gas avoids the nucleus; higher speeds are observed at larger radii, indicating outflow. The black dotted circles show the locations of the X-ray bubbles. The molecular gas appears to be drawn up behind the rising bubbles. (A color version of this figure is available in the online journal.)

or that it arrived provenance unknown and is supported against gravity by orbiting with a large velocity in the plane of the sky. The former interpretation implies an X-ray cooling rate of $\sim 1000 M_{\odot} \text{ yr}^{-1}$, which is inconsistent with an upper limit from X-ray spectroscopy of $< 140 M_{\odot} \text{ yr}^{-1}$ (Sanders et al. 2010). Neither scenario can be ruled out using the data at hand. However, the velocity patterns and flow rates implied by the CO (3–2) and CO (1–0) emissions are inconsistent with steady inflow and are more naturally interpreted in the context of a bipolar outflow of molecular gas.

4.2. Driving a Molecular Outflow by Radiation Pressure or Supernovae

Molecular outflows are common in ULIRGs, QSOs, and starburst galaxies (reviewed by Veilleux et al. 2005 and Fabian 2013). Driving mechanisms include radiation pressure on dust and mechanical winds powered by supernovae. Radiation from hot stars and AGNs will drive out gas when $dM/dt \times v_{\text{CO}} \lesssim L_{\text{UV}}/c$. The left-hand side is the product of the outflow rate and the gas velocity. The right-hand side is the sum of the UV luminosity from the AGN and stars divided by the speed of light. The FUV image shown in Figure 2 reveals no UV point source associated with the AGN. Stars are producing all of the UV flux. For a stellar UV luminosity $L_{\text{FUV}} = 1.85 \times 10^{43} \text{ erg s}^{-1}$ (O’Dea et al. 2010), radiation pressure would be too feeble to drive an outflow rate of $200 M_{\odot} \text{ yr}^{-1}$ by more than three orders of magnitude.

The power input by core collapse supernovae, $4 \times 10^{43} \text{ erg s}^{-1}$ (M06), is comparable to the kinetic power of the outflow, $E_{\text{K}} \simeq 10^{58} \text{ erg}$, $t_{\text{out}} \simeq 3 \times 10^7 \text{ yr}$, $P_{\text{K}} \sim 10^{43} \text{ erg s}^{-1}$, and is therefore energetically significant. However, in order to power the flow by supernova explosions, most of their mechanical energy must couple to molecular gas driving bulk motion rather than thermal motion, which would be hard to understand. Furthermore, their spherical blast patterns and the work against gravity and

the surrounding gas pressure would hinder a sustained and substantial bipolar flow over such large distances. Instead of driving a flow, supernova explosions may be thickening the disk and perhaps increasing the cross section between the molecular gas and the radio AGN, which can easily power the flow (Section 4.4).

4.3. A Radio-AGN Driving a Molecular Outflow

The mechanical power of the jet estimated from the X-ray cavities, $P_{\text{cav}} \simeq 10^{45} \text{ erg s}^{-1}$, is by far the most potent power source. Although the jet momentum is insufficient to lift the gas, the kinetic energy of the cold flows is only $\sim 1\%$ of the total energy output of the AGN. The molecular gas is projected along and behind the rising bubbles, providing circumstantial evidence connecting the bubbles to the molecular flow. Moreover, the molecular flow speeds are consistent with buoyancy speeds of cavities, which rise at a substantial fraction of the atmosphere’s sound speed (Churazov et al. 2001). The atmospheric sound speed in A1835 is $\sim 1000 \text{ km s}^{-1}$.

This interpretation has its own problems. Despite ample AGN power, the bubbles must couple to the molecular gas and lift it out of the galaxy. By Archimedes’ principle, they would be unable to lift more molecular gas than hot gas they displace, which is $\sim 3 \times 10^{10} M_{\odot}$. In addition to displacing the hot plasma, rising X-ray bubbles draw metal-enriched X-ray plasma out from cluster centers at rates of tens to hundreds of solar masses per year (Simionescu et al. 2008; Werner et al. 2010; Kirkpatrick et al. 2009, 2011). A1835’s AGN is lifting $\sim 4 \times 10^{10} M_{\odot}$ of hot gas out along the bubble axis (C. C. Kirkpatrick, in preparation), a value that is a few times larger than the mass of the molecular outflow and close to our estimate of the amount of gas displaced by the bubbles. These estimates are uncomfortably close to the outflowing molecular gas mass and would imply surprisingly efficient coupling between the radio bubbles and both the hot,

$\sim 4 \times 10^7$ K, tenuous, 0.1 cm^{-3} , volume-filling plasma and the ~ 30 K molecular gas.

How the molecular gas couples to the bubbles is unclear. Ram pressure associated with simulated high-Eddington-ratio hydrodynamic jets is able to sweep away both the cold and warm phases of the interstellar medium (e.g., Wagner et al. 2012). Whether the molecular clouds in A1835 are being accelerated by jets or are being lifted in the updraft of the X-ray bubbles (e.g., Pope et al. 2010) is unclear. Observation suggests the latter. Molecular gas is more readily coupled to the hot gas when the density contrast is low. In Section 4.4, the density in the molecular disk is estimated to be ~ 1000 times that of the hot phase. However, for turbulent velocities of $\sim 100 \text{ km s}^{-1}$, if the dynamical pressure of the molecular gas matched the pressure of the hot gas, it would only be 50 times as dense. The high level of turbulence maintained by rapid ongoing star formation may then help to explain how the tenuous hot gas is able to lift molecular gas.

The bubbles would be able to lift the mass more easily if the molecular hydrogen cooled out of hotter gas as it rises in the bubbles' wake (see, for example, Revaz et al. 2008). The mean plasma density and temperature in the central 20 kpc of the cluster are 0.1 cm^{-3} and $T = 2.5 \text{ keV}$, respectively. The cooling time of this gas, assuming solar metal abundance, is 0.22 Gyr, which is longer than the time it would take to displace the gas to a projected distance of about 10 kpc. However, lower entropy gas at a temperature of 1 keV in local pressure equilibrium would have a density of 0.25 cm^{-3} . Its cooling time would be only 2×10^7 yr, which is comparable to the rise times of both the bubbles and molecular gas. Therefore, the $\lesssim 1$ keV plasma lifted out of the center would have time to cool behind the cavities. This rapidly cooling plasma would have densities a few times larger than the ambient plasma, but it would be several orders of magnitude less dense than the molecular gas itself. It would therefore be much easier to lift and accelerate to the speeds observed. This mechanism, which would tend to draw the most rapidly cooling plasma out of the BCG, may help to explain the dearth of $\lesssim 1$ keV plasma in A1835 and other clusters (Peterson et al. 2003).

The outflow rate is a poorly defined quantity. We estimate it by dividing the mass of the outflowing molecular gas by either the time for the bubbles to rise by buoyancy to their current projected distances or by the time required for the molecular gas to reach its current projected distance from the nucleus. A range of velocities and distances are observed, with timescales lying between $3\text{--}5 \times 10^7$ yr. They imply an outflow rate of $\sim 200\text{--}300 M_\odot \text{ yr}^{-1}$, which is comparable to the BCG's mean star formation rate. The center of the galaxy would then be swept of its molecular gas in only a few hundred million years, starving the black hole and starburst of needed fuel. However, the fate of most of the gas is unclear. The one-dimensional outflow speeds are somewhat larger than the circular speed of the stars. If the molecular gas is flowing ballistically, most of it should return unless it evaporates into the hot atmosphere. If the molecular gas is coupled to the rising bubbles or continues to be accelerated by the AGN, it could travel further. However, if the molecular gas formed behind the bubbles in a cooling wake, it is unlikely to evaporate into the hot medium and would return in a circulation flow or "fountain" of molecular gas, similar to that inferred in NGC 1275 (Lim et al. 2008; Salomé et al. 2006, 2011). The impact of a molecular fountain on the star formation and AGN histories of BCGs and normal elliptical galaxies is not understood.

4.4. Dynamics of the Central Molecular Gas

The dynamical state and high average density of the molecular gas in the central kiloparsec of the BCG have significant implications for this system. The lack of evidence for rotation in the molecular gas implies that, if the gas is rotationally supported, its rotation axis must be very close to our line of sight. At the same time, the full velocity width at half maximum for the molecular gas in this region is 130 km s^{-1} , corresponding to a line-of-sight velocity dispersion of $\sigma_{\text{los}} \simeq 55 \text{ km s}^{-1}$ and a one-dimensional turbulent velocity $v_T = \sigma_{\text{los}}$. This suggests the gas lies in a face-on disk.

This high turbulent velocity is consistent with the disk being marginally gravitationally unstable; the Toomre Q parameter is

$$Q = \frac{v_c v_T}{\pi G r \Sigma_g(r)} \approx 0.43 \left(\frac{v_c}{400 \text{ km s}^{-1}} \right) \left(\frac{v_T}{55 \text{ km s}^{-1}} \right) \times \left(\frac{R_e}{2 \text{ kpc}} \right)^{-1} \left(\frac{\Sigma_g(R_e)}{0.4 \text{ g cm}^{-2}} \right)^{-1}, \quad (2)$$

where we have scaled to the radius R_e enclosing half the CO (3–2) flux, which we assume to enclose half the mass. Based on A1835's mass profile (R. A. Main et al., in preparation; see Section 4.1), the circular speed at 10 kpc lies between 300 and 420 km s^{-1} .

We have therefore scaled the circular velocity at 2 kpc to a conservative value of 400 km s^{-1} . The circular velocity would have to exceed 940 km s^{-1} to stabilize the gas disk, so the Toomre criterion is easily met. We noted in Section 3.2 that the BCG lies with starburst galaxies on the Schmidt–Kennicutt relation; galaxies on that relation have $Q \lesssim 1$. Furthermore, A1835's disk has similar properties to those observed in vigorously star-forming galaxies at $z \sim 2$ (e.g., Elmegreen & Elmegreen 2006; Newman et al. 2012).

For a gas-to-dust mass ratio of 100, the surface density ($\Sigma_g = 1600 M_\odot \text{ pc}^{-2}$) corresponds to an $A_v \approx 100$. The weight per unit area under self-gravity or dynamical pressure of this gas is

$$p_{\text{dyn}} = \frac{\pi}{2} G \Sigma_g^2 \approx 1.7 \times 10^{-8} \text{ dyne cm}^{-2}. \quad (3)$$

This is substantially higher than the thermal pressure of the hot gas.

Being marginally gravitationally stable implies that the disk scale height $H = (v_T/v_c)r$, or about 275 pc at $R_e = 2$ kpc. The mean density at that radius is then $\bar{\rho}_c = \Sigma_g/(2H) \approx 2.4 \times 10^{-22} \text{ g cm}^{-3}$, or $n_H \approx 100$. This mean density is somewhat higher than the mean density in massive Milky Way giant molecular clouds. The Toomre mass of molecular clouds is then $M_T = H^2 \Sigma_g \simeq 1.4 \times 10^8 M_\odot$. The turbulent pressure of the cold gas is

$$p_{\text{turb}} = \bar{\rho}_c v_T^2 \approx 0.7 \times 10^{-8} \text{ dyne cm}^{-2}, \quad (4)$$

i.e., the turbulent motions provide enough pressure to support the disk in a marginally stable state.

Turbulence is believed to decay on a dynamical time. Maintaining the turbulence in A1835 would then require a turbulent power of

$$P_{\text{turb}} = \frac{3M_g v_T^2}{2R_e/v_c} \simeq 3 \times 10^{43} \text{ erg s}^{-1}.$$

This is similar to the total luminosity supplied by supernovae, if the star formation rate is $\sim 200 M_\odot \text{ yr}^{-1}$, $L_{\text{Sne}} =$

$6 \times 10^{43} (\dot{M}_*/200 M_\odot \text{ yr}^{-1}) \text{ erg s}^{-1}$, if the supernovae are well coupled to the molecular gas and if they do not radiate more than $\sim 50\%$ of their energy away. We observe that $Q \approx 1$, so we expect large-scale features such as spiral arms or bars in the disk to develop. These features will transport angular momentum efficiently inward, down to subparsec scales, e.g., Hopkins & Quataert (2010, 2011).

4.5. Origin of the Molecular Gas

Molecular gas associated with starburst galaxies, ULIRGS, and QSOs is often attributed to wet mergers. The center of a rich cluster with a large velocity dispersion and a dearth of gas-rich donor galaxies is an unlikely location for a wet merger. Ram pressure experienced by a plunging, gas-rich donor galaxy would strip most of its atomic gas and much of its molecular gas before it reaches the BCG (Combes 2004; Roediger & Brüggén 2007; Kirkpatrick et al. 2009; Ruszkowski et al. 2012). Being dense and centrally concentrated, molecular gas is tightly bound and more resilient to stripping than atomic gas. Therefore, short of a direct collision, a plunging galaxy should retain much of its molecular gas (Young et al. 2011). Finally, the BCG’s molecular gas mass exceeds by large factors that of most galaxies in clusters at its epoch. The likelihood that such a galaxy, if present, would hit the BCG directly and deposit its molecular gas at the low speeds observed seems remote.

The molecular gas in A1835 probably cooled from the hot atmosphere and settled into the BCG. Molecular gas masses of 10^9 – $10^{10} M_\odot$ are prevalent in BCGs but only those centered in hot atmospheres whose central cooling times lie below $\sim 10^9$ yr (Edge 2001; Salomé & Combes 2003). BCGs in Coma-like clusters with long central cooling times are not gas rich. A1835 is an extreme example of this class of BCGs. Its cooling rate of $\lesssim 140 M_\odot \text{ yr}^{-1}$ (Sanders et al. 2010) would supply the molecular gas in a few hundred Myr, which is comparable to the age of the starburst (M06).

5. CONCLUSIONS

We have shown that the BCG in A1835 contains roughly $5 \times 10^{10} M_\odot$ of molecular gas, most of which is associated with stars forming at a rate of 100 – $180 M_\odot \text{ yr}^{-1}$, in a thick, turbulent disk projected face-on. We discovered a $\sim 10^{10} M_\odot$ bipolar molecular flow traveling between -250 and $+480 \text{ km s}^{-1}$ that we suggest is being accelerated outward by mechanical energy associated with rising X-ray bubbles. Whether the bubbles accelerated the molecular clouds themselves or whether the molecular clouds cooled out of the hot plasma in the updraft behind the bubbles is unclear. We highlight the difficulty of lifting dense molecular gas out of the central disk and we propose that the molecular gas in the flow may have cooled in the updraft of hot plasma behind the bubbles. The problem would be mitigated if the outflowing mass were lower than we have estimated, for example, if the X_{CO} parameter were lower than the value we assumed.

Our result has broader implications. Molecular gas abundance is a sharply declining function of a galaxy’s stellar mass. Above $3 \times 10^{10} M_\odot$ most are elliptical galaxies. Of these, only $\sim 22\%$ contain molecular gas, and only at levels between 10^7 and $10^9 M_\odot$ (Young et al. 2011). In contrast, radio power is a steeply increasing function of stellar mass (Best et al. 2005; Best & Heckman 2012). Their radio detection fraction rises from 0.01% at $3 \times 10^{10} M_\odot$ to upward of 30% at $5 \times 10^{11} M_\odot$ (Best et al. 2005). Therefore, molecular gas mass must also

be a declining function of radio power. While a number of environmental factors may be contributing to this decline (Young et al. 2011), the radio source itself may play a role, albeit a complex one. Radio synchrotron power represents only a small fraction of a radio AGN’s total mechanical power (Birzan et al. 2008). Therefore, relatively low-power radio synchrotron sources can be mechanically potent. Mechanical heating of hot atmospheres in elliptical galaxies by radio-mode feedback is likely to be the primary mechanism maintaining “red and dead” elliptical galaxies (e.g., Bower et al. 2006; Croton et al. 2006). However, radio AGNs are likely fed by cold clouds. A feedback loop may be difficult to sustain unless the radio jets are also affecting the rate of cold gas accretion by driving it away from the nucleus. The relatively efficient coupling between the molecular gas and radio bubbles inferred here in A1835 and in other radio galaxies (e.g., Morganti et al. 2005) suggests that radio-mode feedback may also be regulating the amount of molecular gas reaching the centers of galaxies.

B.R.M. thanks Tom Jones and Christine Jones for helpful comments. H.R.R. and B.R.M. acknowledge generous financial support from the Canadian Space Agency Space Science Enhancement Program. B.R.M., R.A.M., H.R.R., and A.N.V. acknowledge support from the Natural Sciences and Engineering Research Council of Canada. A.C.E. acknowledges support from STFC grant ST/I001573/1. P.E.J.N. is supported by NASA grant NAS8-03060. We thank the ALMA scientific support staff members Adam Leroy and Stéphane Leon. The paper makes use of the following ALMA data: ADS/JAO.ALMA No. 2011.0.00374.S. ALMA is a partnership of ESO (representing its member states), NSF (USA), and NINS (Japan), with NRC (Canada) and NSC and ASIAA (Taiwan), in cooperation with the Republic of Chile. The Joint ALMA Observatory is operated by ESO, AUI/NRAO, and NAOJ. The National Radio Astronomy Observatory is a facility of the National Science Foundation operated under cooperative agreement by Associated Universities, Inc. This paper is dedicated to Jim Pisano, who helped make ALMA the marvelous facility it is.

APPENDIX

THE CO TO H_2 CONVERSION FACTOR

CO traces molecular hydrogen which, lacking a permanent electric dipole moment, radiates inefficiently. The value of the CO to molecular gas conversion factor, commonly referred to as X_{CO} , is the prime uncertainty in our mass estimates. Absent an alternative, most investigators adopt the value for the Milky Way Galaxy and other local disk galaxies, where the CO (1–0) emission feature is usually optically thick. However, the true value depends on environmental factors, such as the gas-phase metal abundance, which may depart from the average Galactic value. A lower gas-phase metal abundance gives a higher mass ratio of hydrogen to CO. Therefore, applying the Galactic X_{CO} to gas with low metal abundance would underestimate the total molecular gas mass. Conversely, if the molecular gas is optically thin or nearly so, as it may be in turbulent flows and massive starburst galaxies, the Galactic X_{CO} would overestimate the molecular gas mass. Other factors that affect X_{CO} include the temperature, density, and dynamics of the gas, which in most situations are poorly understood (Bolatto et al. 2013).

The metallicity of the cooling X-ray plasma in A1835 lies between 0.5 and 0.8 times the Solar metallicity within 20 kpc of the nucleus. This alone would indicate that adopting the

Galactic X_{CO} as we have done should provide a reasonable if not a conservative underestimate of the molecular gas mass. However, A1835 is a starburst galaxy. There are indications that X_{CO} in starburst galaxies may be depressed below the Galactic value. The central gas density, $\sim 2000 M_{\odot} \text{pc}^{-2}$, lies midway between normal spirals and starbursts. The gas density of the outflow, away from the bulk of star formation, has a surface density of $\sim 100 M_{\odot} \text{pc}^{-2}$, which is comparable to normal spiral galaxies and to the Milky Way (Bolatto et al. 2013). It is therefore possible that the X_{CO} value for the molecular gas located near the nucleus may be suppressed by a small factor with respect to the molecular gas in the outflow. In contrast, indications are that X_{CO} may be suppressed in turbulent winds where the molecular gas becomes optically thin (Bolatto et al. 2013). A1835's outflow velocity is lower than those in quasars (e.g., Maiolino et al. 2012; Feruglio et al. 2010). Taken together, we have no reason to expect X_{CO} to depart significantly from the Galactic value in this system. Nevertheless, should X_{CO} lie a factor of several below the Galactic value, the flow would still exceed $10^9 M_{\odot}$. This would not qualitatively alter our result.

REFERENCES

- Best, P. N., & Heckman, T. M. 2012, *MNRAS*, 421, 1569
 Best, P. N., Kauffmann, G., Heckman, T. M., et al. 2005, *MNRAS*, 362, 25
 Bîrzan, L., McNamara, B. R., Nulsen, P. E. J., Carilli, C. L., & Wise, M. W. 2008, *ApJ*, 686, 859
 Bolatto, A. D., Wolfire, M., & Leroy, A. K. 2013, *ARA&A*, 51, 207
 Bower, R. G., Benson, A. J., Malbon, R., et al. 2006, *MNRAS*, 370, 645
 Cavagnolo, K. W., Donahue, M., Voit, G. M., & Sun, M. 2008, *ApJL*, 683, L107
 Churazov, E., Brüggen, M., Kaiser, C. R., Böhringer, H., & Forman, W. 2001, *ApJ*, 554, 261
 Combes, F. 2004, in IAU Symp. 217, Recycling Intergalactic and Interstellar Matter, ed. P.-A. Duc, J. Braine, & E. Brinks (San Francisco, CA: ASP), 440
 Crawford, C. S., Allen, S. W., Ebeling, H., Edge, A. C., & Fabian, A. C. 1999, *MNRAS*, 306, 857
 Croton, D. J., Springel, V., White, S. D. M., et al. 2006, *MNRAS*, 365, 11
 Donahue, M., de Messières, G. E., O'Connell, R. W., et al. 2011, *ApJ*, 732, 40
 Edge, A. C. 2001, *MNRAS*, 328, 762
 Egami, E., Misselt, K. A., Rieke, G. H., et al. 2006, *ApJ*, 647, 922
 Elmegreen, B. G., & Elmegreen, D. M. 2006, *ApJ*, 650, 644
 Emonts, B. H. C., Norris, R. P., Feain, I., et al. 2013, *MNRAS*, 438, 2898
 Fabian, A. C. 1994, *ARA&A*, 32, 277
 Fabian, A. C. 2013, *ARA&A*, 50, 455
 Feruglio, C., Maiolino, R., Piconcelli, E., et al. 2010, *A&A*, 518, L155
 Gaspari, M., Ruszkowski, M., & Oh, S. P. 2013, *MNRAS*, 432, 3401
 Gaspari, M., Ruszkowski, M., & Sharma, P. 2012, *ApJ*, 746, 94
 Guo, F., & Mathews, W. G. 2013, *ApJ*, 780, 126
 Heckman, T. M. 1981, *ApJL*, 250, L59
 Hopkins, P. F., & Quataert, E. 2010, *MNRAS*, 407, 1529
 Hopkins, P. F., & Quataert, E. 2011, *MNRAS*, 415, 1027
 Hu, E. M., Cowie, L. L., & Wang, Z. 1985, *ApJS*, 59, 447
 Kennicutt, R. C., Jr. 1998, *ApJ*, 498, 541
 Kirkpatrick, C. C., Gitti, M., Cavagnolo, K. W., et al. 2009, *ApJL*, 707, L69
 Kirkpatrick, C. C., McNamara, B. R., & Cavagnolo, K. W. 2011, *ApJL*, 731, L23
 Lim, J., Ao, Y., & Dinh-V-Trung 2008, *ApJ*, 672, 252
 Maiolino, R., Gallerani, S., Neri, R., et al. 2012, *MNRAS*, 425, L66
 McDonald, M., Bayliss, M., Benson, B. A., et al. 2012, *Natur*, 488, 349
 McNamara, B. R., & Nulsen, P. E. J. 2007, *ARA&A*, 45, 117
 McNamara, B. R., & Nulsen, P. E. J. 2012, *NJP*, 14, 055023
 McNamara, B. R., Rafferty, D. A., Bîrzan, L., et al. 2006, *ApJ*, 648, 164
 Morganti, R., Fogasy, J., Paragi, Z., Oosterloo, T., & Orienti, M. 2013, *Sci*, 341, 1082
 Morganti, R., Tadhunter, C. N., & Oosterloo, T. A. 2005, *A&A*, 444, L9
 Narayanan, D., Krumholz, M. R., Ostriker, E. C., & Hernquist, L. 2012, *MNRAS*, 421, 3127
 Nesvadba, N. P. H., Lehnert, M. D., Eisenhauer, F., et al. 2006, *ApJ*, 650, 693
 Newman, S. F., Shapiro Griffin, K., Genzel, R., et al. 2012, *ApJ*, 752, 111
 O'Dea, C. P., Baum, S. A., Privon, G., et al. 2008, *ApJ*, 681, 1035
 O'Dea, K. P., Quillen, A. C., O'Dea, C. P., et al. 2010, *ApJ*, 719, 1619
 O'Neill, S. M., & Jones, T. W. 2010, *ApJ*, 710, 180
 Peterson, J. R., & Fabian, A. C. 2006, *PhR*, 427, 1
 Peterson, J. R., Kahn, S. M., Paerels, F. B. S., et al. 2003, *ApJ*, 590, 207
 Pizzolato, F., & Soker, N. 2010, *MNRAS*, 408, 961
 Pope, E. C. D., Babul, A., Pavlovski, G., Bower, R. G., & Dotter, A. 2010, *MNRAS*, 406, 2023
 Rafferty, D. A., McNamara, B. R., & Nulsen, P. E. J. 2008, *ApJ*, 687, 899
 Revaz, Y., Combes, F., & Salomé, P. 2008, *A&A*, 477, L33
 Roediger, E., & Brüggen, M. 2007, *MNRAS*, 380, 1399
 Russell, H. R., McNamara, B. R., Edge, A. C., et al. 2014, *ApJ*, 784, 78
 Ruszkowski, M., Brüggen, M., Lee, D., & Shin, M.-S. 2012, arXiv:1203.1343
 Salomé, P., & Combes, F. 2003, *A&A*, 412, 657
 Salomé, P., Combes, F., Edge, A. C., et al. 2006, *A&A*, 454, 437
 Salomé, P., Combes, F., Revaz, Y., et al. 2011, *A&A*, 531, A85
 Sanders, J. S., Fabian, A. C., Smith, R. K., & Peterson, J. R. 2010, *MNRAS*, 402, L11
 Simionescu, A., Werner, N., Finoguenov, A., Böhringer, H., & Brüggen, M. 2008, *A&A*, 482, 97
 Villeux, S., Cecil, G., & Bland-Hawthorn, J. 2005, *ARA&A*, 43, 769
 Villar-Martín, M., Sánchez, S. F., De Breuck, C., et al. 2006, *MNRAS*, 366, L1
 Voit, G. M. 2011, *ApJ*, 740, 28
 Voit, G. M., Cavagnolo, K. W., Donahue, M., et al. 2008, *ApJL*, 681, L5
 Wagner, A. Y., Bicknell, G. V., & Umemura, M. 2012, *ApJ*, 757, 136
 Werner, N., Simionescu, A., Million, E. T., et al. 2010, *MNRAS*, 407, 2063
 Wilman, R. J., Edge, A. C., & Swinbank, A. M. 2006, *MNRAS*, 371, 93
 Young, L. M., Bureau, M., Davis, T. A., et al. 2011, *MNRAS*, 414, 940